Journal of Science: Advanced Materials and Devices 1 (2016) 367–378

Contents lists available at ScienceDirect

Journal of Science: Advanced Materials and Devices

journal homepage: www.elsevier.com/locate/jsamd

Original Article

Design and characterization of non-toxic nano-hybrid coatings for corrosion and fouling resistance

P. Saravanan [a, *], K. Jayamoorthy [a], S. Ananda Kumar [b]

[a] Department of Chemistry, St. Joseph's College of Engineering, Chennai 600119, Tamil Nadu, India
[b] Department of Chemistry, Anna University, Chennai 600 025, Tamil Nadu, India

ARTICLE INFO

Article history:
Received 23 June 2016
Received in revised form
4 July 2016
Accepted 4 July 2016
Available online 11 July 2016

Keywords:
Epoxy
Nano-hybrid coatings
Anticorrosion
Antimicrobial
Antifouling

ABSTRACT

Epoxy resin modified with nano scale fillers offers excellent combination of properties such as enhanced dimensional stability, mechanical and electrical properties, which make them ideally suitable for a wide range of applications. However, the studies about functionalized nano-hybrid for coating applications still require better insight. In the present work we have developed silane treated nanoparticles and to reinforce it with diglycidyl epoxy resin to fabricate surface functionalized nano-hybrid epoxy coatings. The effect of inorganic nano particles on the corrosion and fouling resistance properties was studied by various (1, 3, 5 and 7 wt%) filler loading concentrations. Diglycidyl epoxy resin (DGEBA) commonly was used for coating. 3-Aminopropyltriethoxysilane (APTES) was used as a coupling agent to surface treats the TiO_2 nanoparticles. The corrosion and fouling resistant properties of these coatings were evaluated by electrochemical impedance and static immersion tests, respectively. Nano-hybrid coating (3 wt% of APTES–TiO_2) showed corrosion resistance up to 10^8 Ω cm^2 after 30 days immersion in 3.5% NaCl solution indicating an excellent corrosion resistance. Static immersion test was carried out in Bay of Bengal (Muttukadu) which has reflected good antifouling efficiency of the 3 wt% APTES–TiO_2 loaded nano-hybrid coating up to 6 months.

1. Introduction

In recent years, with the development of nano technology, researchers try using nano size fillers to modify epoxy resins. The nanoparticle reinforced epoxy resins show huge improvements on their properties due to the unique characters of nano size fillers [1,2]. Currently people believe that the improvements of epoxy resins' properties are the result of nano size particles' surface effect, quantum size effect and macroscopic quantum tunneling effect [3]. Because of the high viscidity of epoxy resin, it is hard to mix nano size fillers uniformly into epoxy resins. So it is also necessary to consider the manufacture process. Corrosion protection of metallic substrates was one of the important roles performed by organic coatings. Such coatings remain cost-effective for many users who would like to have substrates coated just once and assume appearance and function to be maintained. Organic coatings are often used as a protective layer over the metal substrate to prevent the substrate from oxidizing in a manner deleterious to the function and appearance of an object. They do so in several ways [4]. First, they act as a barrier limiting the passage of current necessary to connect the areas of anodic and cathodic activity on the substrate. This occurs especially if the coating wets the substrate surface very well and has good adhesion in the presence of water and electrolyte. Coatings do not really stop oxygen sufficiently to make concentrations at the surface rate limiting and they do not completely stop water ingress into them. However, a good barrier coating slows water and electrolyte penetrations and is not displaced by water at the substrate/coating interface.

Furthermore, the barrier performance of epoxy coatings can be enhanced by the incorporation of a second phase that is miscible with the epoxy polymer, by decreasing the porosity and zigzagging the diffusion path for deleterious species. For instance, inorganic filler particles at nanometer scale can be dispersed within the epoxy resin matrix to form an epoxy nano-hybrid coating. The incorporation of nanoparticles into epoxy resins offers environmentally benign solutions to enhance the integrity and durability of coatings, since the fine particles dispersed thoroughly in coatings can fill cavities [5–7] and cause crack bridging, crack deflection and crack bowing [8]. Nanoparticles can also prevent epoxy

* Corresponding author.
E-mail address: profsaran1@gmail.com (P. Saravanan).
Peer review under responsibility of Vietnam National University, Hanoi.

http://dx.doi.org/10.1016/j.jsamd.2016.07.001

disaggregation during curing, resulting in a more homogenous coating. Nanoparticles tend to occupy small hole defects formed from local shrinkage during curing of the epoxy resin and act as a bridge interconnecting more molecules. This results in a reduced total free volume as well as an increase in the cross-linking density [9,10], In addition, epoxy coatings containing nanoparticles offer significant barrier properties for corrosion protection [11,12] and reduce the trend for the coating to blister or delaminate.

In recent years, a rapid surge of "green" metal pre-treatment technology based on the silane agents was found in the field of corrosion control of metals. The silane coupling agents have a general structure of $(XO)_3SiY$, where XO is a hydrolyzable alkoxy group, which can be methoxy (OCH_3) or ethoxy (OC_2H_5) and Y is an organofuctional group. The formation of silane films is based on the condensation reactions between silanols (Si-OH, hydrolysis product of alkoxy group) and the metal hydroxyls (Me-OH). The organofuntional silane films deposited on the metal are usually hydrophobic. They can act as a physical barrier against water. In addition, the silane films can also act as adhesion promoters between metal substrate and organic coatings. In the past decade many studies were done in corrosion protection properties of such silane films [13–15].

In addition to the anticorrosion properties of epoxy nanohybrid coatings they have enhanced an antimicrobial property that is useful in marine applications. Marine microbiological corrosions are responsible for considerable damages to all devices and vessels immersed in seawater, and this induces serious economic problem to maritime activities [16]. Employing effective antifouling marine paints, containing booster biocides at non-toxic levels is one approach to solve the issue of fouling [17]. One important function of paints containing biocides or inhibitors is to obtain optimal release rate of the actual active substance into the sea. The leaching rate of biocides should not be too fast, resulting in rapid and premature depletion of the antifouling activity of marine coatings and unnecessarily high concentration in the sea. However, the release rate should not be too slow since this would undoubtedly result in fouling [18]. In order to deal with both issues, application of core–shell structured materials should be one of the best alternatives since the shells offer protection to the cores and introducing new properties to the hybrid structures [19]. With all these thoughts in our mind, we made an attempt to develop a unique epoxy coating formulation having functionalized nano scale filler reinforcement capable of offering both corrosion and microbial prevention.

2. Experimental

2.1. Materials

The base materials used in this work are di functional epoxy resin (DGEBA) and Aradur HY951 triethylenetetramine (TETA) – a room temperature curing agent, which is used in all the systems supplied by Huntsman Advanced Materials. 3-aminopropyltriethoxysilane and all other reagents were purchased from Sigma–Aldrich chemicals and used without further purification.

2.2. Methods

The FTIR spectra were recorded on a Perkin Elmer 781 FTIR spectrometer that determines the chemical bonds on TiO_2 and APTES. Spectra of nano-hybrid coatings were obtained with KBr pellets. Vibration bands were reported as wave number (cm^{-1}). The TiO_2 particles were characterized by X-ray diffraction (XRD) was equipped with a Copper target ($\lambda = 1.5405$ Å) radiation using Guinier type camera used as focusing geometry and a solid state detector. Curved nickel crystal was used as the monochromator to produce Cu $K_{\alpha 1}$ radiation in the range of 20°–90°. A JEOL JEM-3010 analytical transmission electron microscope, operating at 300 kV with a measured point-to-point resolution of 0.23 nm, was used to characterize the spherical morphology of unmodified TiO_2 and modified TiO_2. The same samples were then coated with a thin layer of gold by vaporization and morphology was observed by scanning electron microscope (LEO 1455VP). Atomic force microscopy (AFM) image of the samples was performed in the air with a digital Instrument AGILENT – NP410A series 5500 AFM in contact mode. Dispersion stability of nanoparticles (untreated and treated) was evaluated in an organic solvent in order to achieve proper dispersion of nanoparticles in the epoxy-based coating and making possible chemical interactions between nanoparticles and polymeric coating. These are then to be subjected to electrochemical impedance and salt-spray analysis to ascertain their corrosion resistance behavior. Isolated microbes and their antimicrobial activity were carried out on epoxy nano-hybrid coatings by agar diffusion technique. Fouling resistance of the coatings was determined by antifouling studies by subjecting the coated samples in sea for a period of 12 months at east coast of India, Tamil Nadu, Chennai (Muttukadu boat house). The interesting results obtained from this investigation are discussed in detail with supporting evidences.

2.3. Synthesis of TiO_2 nanoparticles

For the synthesis of TiO_2, 0.5 M titanium butoxide solution was prepared in 100 ml butanol and stirred for 15 min; further 30 ml DI water was added drop wise in the above solution to allow hydrolysis. This solution was stirred for 30 min, which gave rise to white precipitation. The obtained white precipitate was microwave irradiated for 5 min at 700 W power using microwave system. The microwave used for this experiment was having a power range of 140–700 W. This obtained solution was left 24 h for aging at room temperature and then centrifuged at 2000 rpm for 15 min. Obtained precipitate was dried at 80 °C for 12 h. After complete drying, powder was crushed and calcinated in air at 500 °C for 2 h to remove hydroxide impurities and recrystallization.

2.4. Synthesis of APTES grafted TiO_2 nanoparticles

0.5 g of TiO_2 nanoparticles was dispersed in 50 ml DI water by ultra-sonication for 10 min. Then, the silane coupling agent APTES with concentrations (5 g) were added in the dispersion. After that, dispersed particles were separated from solvent by centrifuge (10 min at 10,000 rpm) followed by washing with ethanol and water alternatively for at least 2 cycles to remove excessive silanes. To re-disperse the centrifuged particles in fresh solvent, they were put in ultrasonic bath for more than 10 min to make sure a visually well dispersed suspension was regained before centrifuge again. Once the process was finished, the modified particles were dried in an oven at 100 °C for 24 h and cooled in a vacuum chamber for 1 h at room temperature.

2.5. Synthesis of TiO_2–APTES–DGEBA nanohybrid coatings

Epoxy coating was prepared using a high speed disperser. The fabrication processes of TiO_2–APTES–DGEBA mixtures were as follows. Different weight percentages of APTES grafted TiO_2 nanoparticle (0, 1, 3, 5 and 7 wt%) were directly added to vessel charged with epoxy resin and solvent mixture (butanol/xylene) followed by addition of additives. The pigment was dispersed by stirring at 400 rotations per minute (RPM) for 30 min and then

Table 1
Nomenclature of coating system on mild steel.

Sample ID	Epoxy resin	Pigment	Surface modified NPs composition (wt%)				Curing agent
			1%	3%	5%	7%	
C1	DGEBA	π	TiO_2	×	×	×	HY951
C2		π	×	TiO_2	×	×	HY951
C3		π	×	×	TiO_2	×	HY951
C4		π	×	×	×	TiO_2	HY951

increasing the stirrer speed to 2000 RPM. The vessel was externally cooled using cold water to avoid rise in temperature during processing. The dispersion was continued for 45–60 min to give a uniform red paint. For curing, epoxy paint and curing agent (HY951) were mixed in a weight ratio 100:58 of epoxy to amine. The mixture was degassed in the vacuum oven for another 20 min at 40 °C to remove any gas bubbles generated during the mixing process. Solvents mixture of xylene and butanol was used for dilution as per the convenience of bar coating application. By this method, different coating formulations were employed for preparation of nano-hybrid coatings and are listed in Table 1. Epoxy coatings with desired thickness were then applied on the sand blasted mild steel substrates using a hand bar film applicator to a thickness of 100 μm. The free-standing films were prepared by application of epoxy nanohybrid coatings on the polystyrene sheets with a film thickness of 100 μm. The films were left for about 2 weeks at room temperature for complete curing. The reaction route of TiO_2–APTES–DGEBA nano-hybrid for coatings is depicted in Fig. 1.

2.6. Surface preparation of mild steel panels for epoxy nano-hybrid coatings

Mild steel (whose chemical compositions are given in Table 2) specimens were used for our study. The different coating systems used to protect steel structures against corrosion were chosen for the purpose of the research. The specimens were degreased with acetone to remove impurities from the substrate. Then the specimens were subjected to sand blasting at a pressure of 100 psi through the nozzle to get the appropriate crevice. The particle size of the sand is 82 meshes. The distance between the substrate and the blaster was maintained 2 feet. The specimens were kept in the desiccator for conditioning. The process of the preparation of hybrid coatings is shown in Fig. 2. Coatings were applied by hand bar coater on commercially available mild steel plates (2 mm × 1 mm × 1 mm) for corrosion resistance test (70 mm × 50 mm × 1 mm) for salt spray test and biofouling test. All the coated samples were cured at room temperature for 3 days and then kept in desiccators for at least 1 week before the tests were performed. Coating thickness was measured by Mini test 600FN, EXACTO-FN type. The thickness of the coatings was found to be approximately ±100 μm. Before subjecting them to various tests, the panels were edge-sealed to an extent of 5–8 mm from the edges using an epoxy type adhesive (supplied by Hindustan Ciba-Geigy Ltd., India).

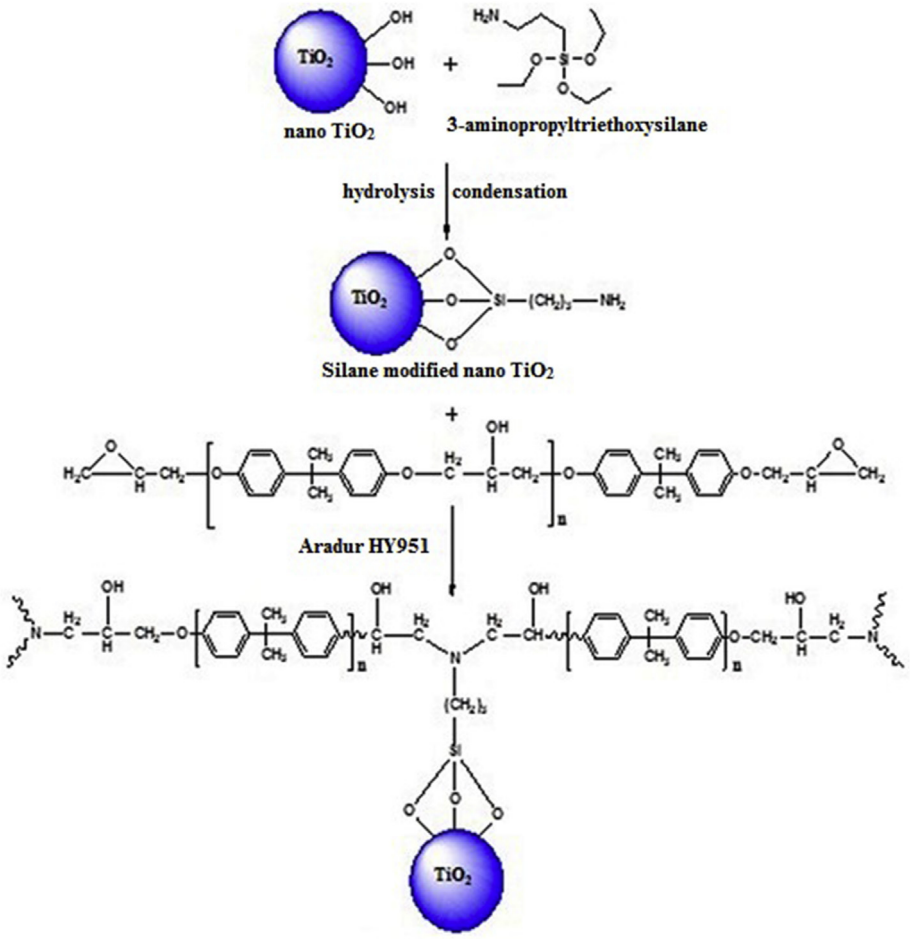

Fig. 1. Synthesis of TiO_2–APTES–DGEBA nano-hybrid for coatings.

Table 2
Chemical composition of mild steel.

Element	C	Si	Mn	P	S	Cr	Ti	Ni	Al	Co	Nb	Fe
Weight (%)	0.033	0.005	0.235	0.011	0.005	0.046	0.003	0.043	0.073	0.007	0.005	Balance

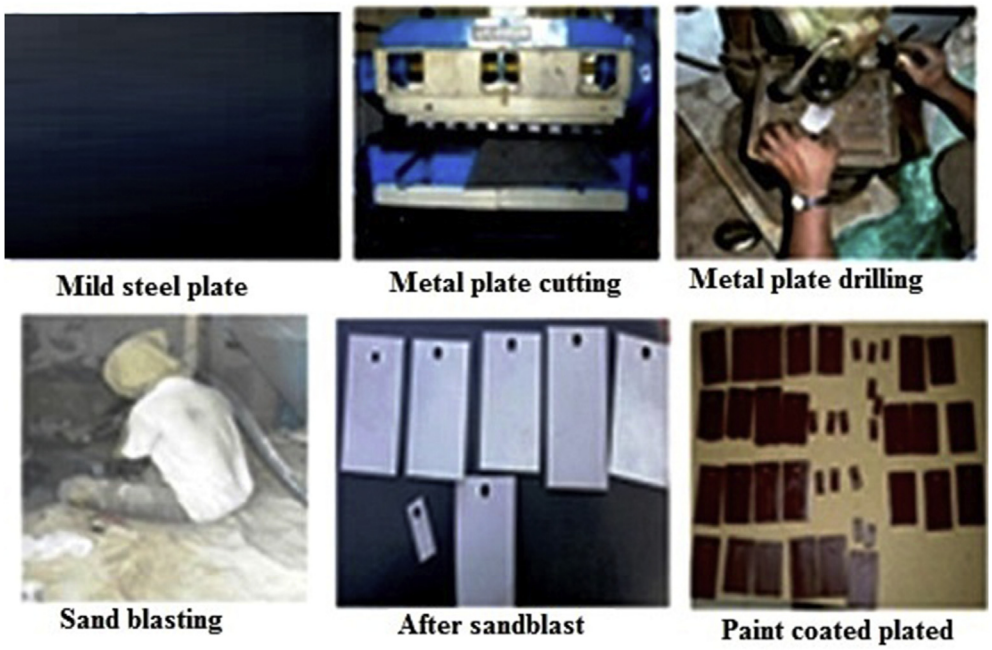

Fig. 2. The process of the preparation of hybrid coatings.

3. Results and discussion

3.1. FTIR spectra of TiO_2 and TiO_2–APTES nanoparticles

The % transmission of APTES, unmodified TiO_2 and APTES grafted TiO_2 by FTIR spectra are shown in Fig. 3. From spectra of modified TiO_2 and unmodified TiO_2, the peaks below 700 cm^{-1}, which were assigned to Ti–O and Ti–O–Ti bonding of titania, were ignored in this case because of their over saturated absorption. The stretching vibration of absorbed water as well as surface hydroxyl groups (OH), which were present in the TiO_2 nanoparticles was confirmed by the broad absorption band between 3400 and 3200 cm^{-1} and the low intensity peak at 1640 cm^{-1}. After surface modification by organosilane, as presented in spectra of modified TiO_2, the asymmetrical and symmetrical stretching vibration of the C–H bond in methylene group was observed at 2928 and 2870 cm^{-1}. Furthermore, the peak corresponding to Si–O–Si bond was observed at around 1040 cm^{-1} indicating the condensation reaction between silanol groups. As shown in Fig. 3, the N–H bending vibration of primary amines (NH_2) was observed as a broad band in the region 1605–1560 cm^{-1}, and another low intensity peak on the shoulder of Titania peak at 1140 cm^{-1} was assigned to the C–N bond. The appearance of these bands demonstrated that amine functional groups in organosilane were grafted onto the modified particle surface. This spectrum reconfirms condensation reaction between methoxy groups of APTES and the TiO_2 surface hydroxyl groups. Since the residual (non-reacted) and physisorbed APTES was removed by extraction in ethanol solution, the mentioned peaks show that grafting of APTES on the nanoparticles has occurred successfully. The hydroxyl groups on the surface of the TiO_2 nanoparticles (Ti-OH) are reactive sites for the reaction with alkoxy groups of silane compounds.

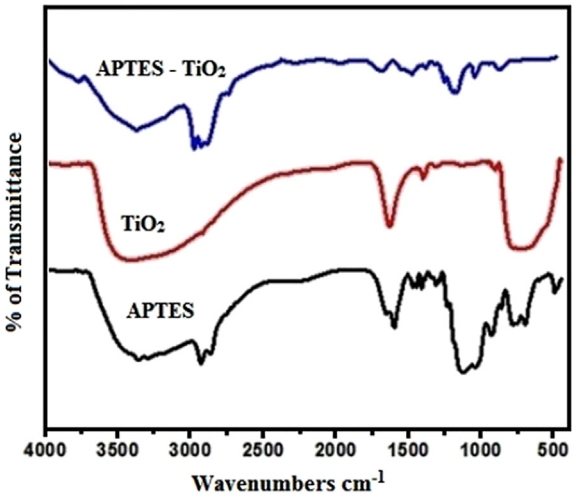

Fig. 3. FTIR spectrum of unmodified TiO_2 NPs, APTES grafted TiO_2 NPs and APTES.

3.2. XRD analysis of TiO_2 and TiO_2–APTES nanoparticles

The X-ray diffraction pattern of the synthesized TiO_2 nanoparticles is shown in Fig. 4a. The obtained diffraction pattern was compared with JCPDS datasheet JCPDS-894921. From Fig. 4a, the 2θ peaks were 25.2, 37.68, 47.84, 54.0, 55.2 and 62.44 were

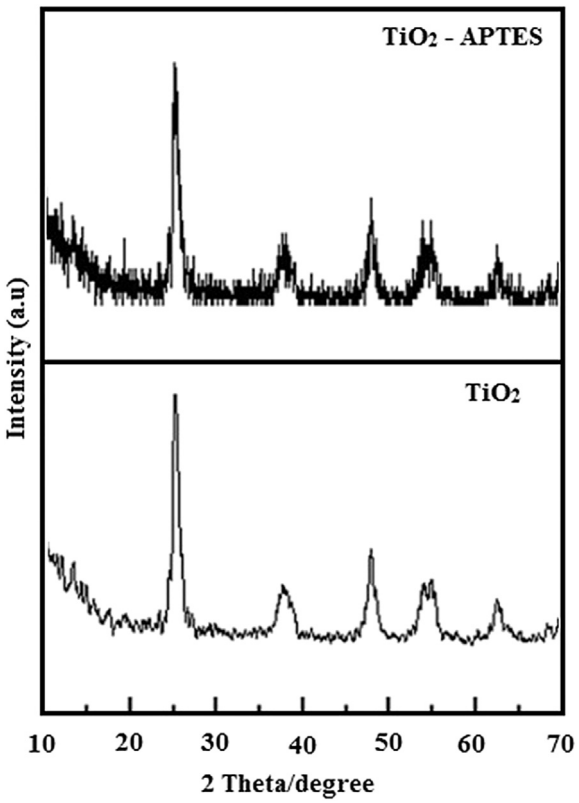

Fig. 4. Powder XRD spectrum of unmodified TiO_2 NPs and APTES grafted TiO_2 NPs.

corresponding to the planes for diffraction with 101, 004, 200, 105, 211 and 213. The crystallite size of nanoparticles was calculated by XRD line broadening of the most intense peak using the Scherrer formula. Crystallite sizes for these nanoparticles are about 35 nm for TiO_2, calculated from the most intense peak. The sharpness of peaks shows that TiO_2 nanoparticles are highly crystalline in nature. The further XRD tests were managed on APTES grafted TiO_2 nanoparticles, the patterns are shown in Fig. 4b as well. The XRD patterns of on APTES grafted TiO_2 nanoparticles are found to be identical to unmodified TiO_2. The comparison of two XRD patterns illustrates that silane group has no impact on the crystal structure of TiO_2.

3.3. Dispersion stability test of TiO_2 and TiO_2–APTES nanoparticles

The results of sedimentation tests of unmodified TiO_2 and APTES grafted TiO_2 NPs suspended in ethanol are shown in Fig. 5. Two types of sedimentation mechanisms could be observed [20], i.e. flocculation and accumulation. For sample containing unmodified TiO_2, the sedimentation mainly occurred by flocculation mechanism. The suspensions separated very quickly into sediments and a clear supernatant on top of the sediment was observed. The separation interfaces between the sediment and the supernatant were sharp and moved downward with time. This sedimentation behavior is typical of flocculated suspensions. For samples APTES grafted TiO_2 nanoparticles the sedimentation was due to their accumulation at the bottom, while columns of cloudy supernatant suspensions still remained after 3 days of settling. Solution containing APTES grafted TiO_2 exhibits the most turbidity. This sedimentation behavior is typical of well-dispersed suspensions and

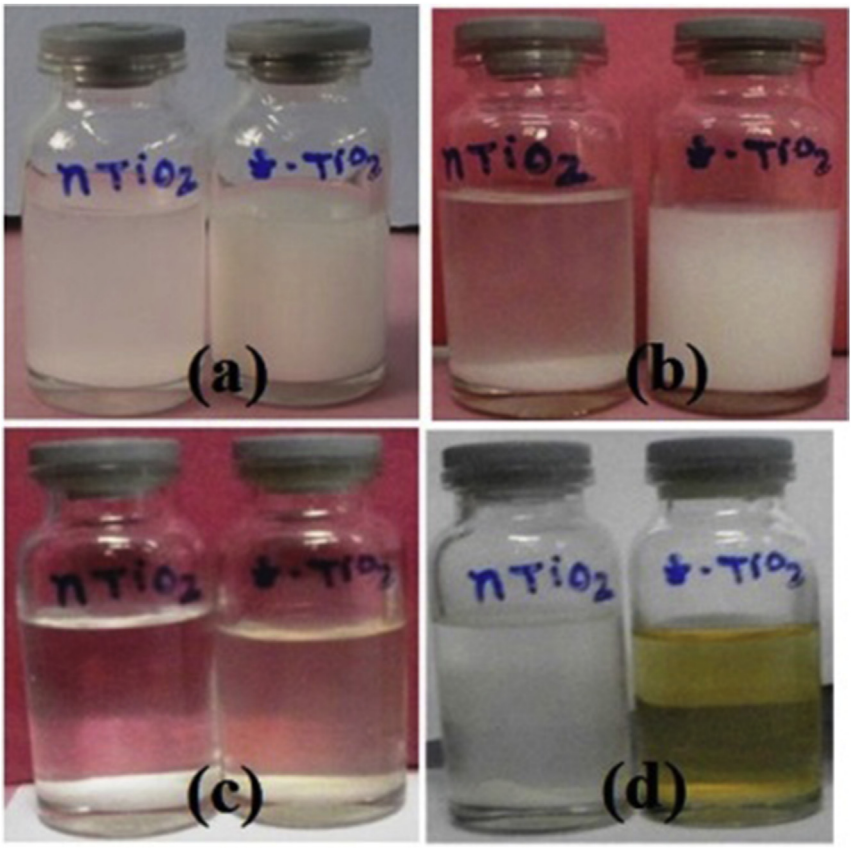

Fig. 5. Dispersion stability of TiO_2 NPs before and after silane surface treatment after (a) 10 min, (b) 24 h, (c) 48 h, (c) 72 h.

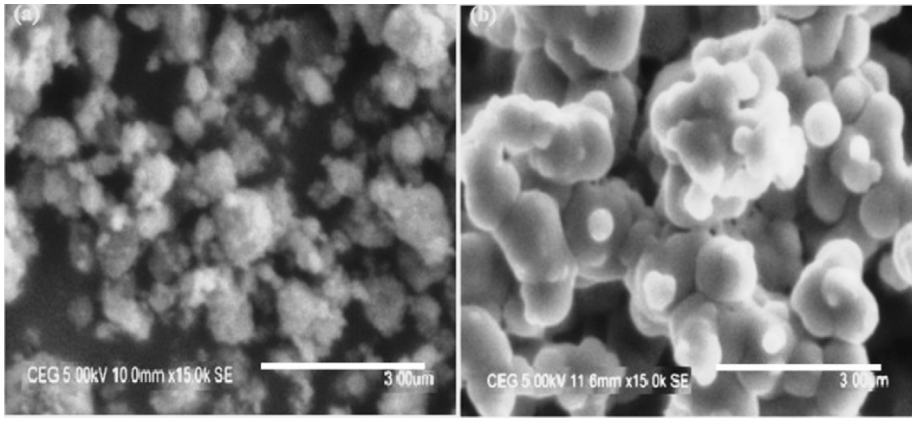

Fig. 6. SEM images of (a) Unmodified TiO_2 NPs, (b) Modified TiO_2 NPs.

smaller particles have much slower settling rates, which might be counter balanced by Brownian motion, they will remain in the supernatant for long times. Even after 3 days the solution containing APTES grafted TiO_2 remained turbid. It clearly indicates that APTES modification can lead to increased stability of nanoparticles in non-polar organic media.

3.4. SEM/EDX, AFM and TEM analysis of TiO_2 and TiO_2–APTES nanoparticles

The morphology of unmodified and modified TiO_2 particles was observed by SEM images. The unmodified TiO_2 particle agglomerated severely as shown in Fig. 6a and separate particles cannot be distinguished. However the EDX analysis suggests the presence of Ti, and oxygen atomic percentage indicates the formation of TiO_2. Moreover, the modified TiO_2 particles shown in Fig. 6b showed different degree of agglomeration; within the agglomerated areas, clear contours are visible between the TiO_2 particles. This indicates that the modified TiO_2 nanoparticles are easier to disperse in the weakly polar media. AFM 3D and topographic image of nanoparticles are shown in Fig. 7a–d. Most of the particles distributed are homogeneous and holds the size less than 53 nm. Fig. 8a & b shows the TEM photograph of TiO_2 nanoparticles before and after treatment. It shows that the particles are of spherical shape. The formation of small aggregates was also noted in the TEM images.

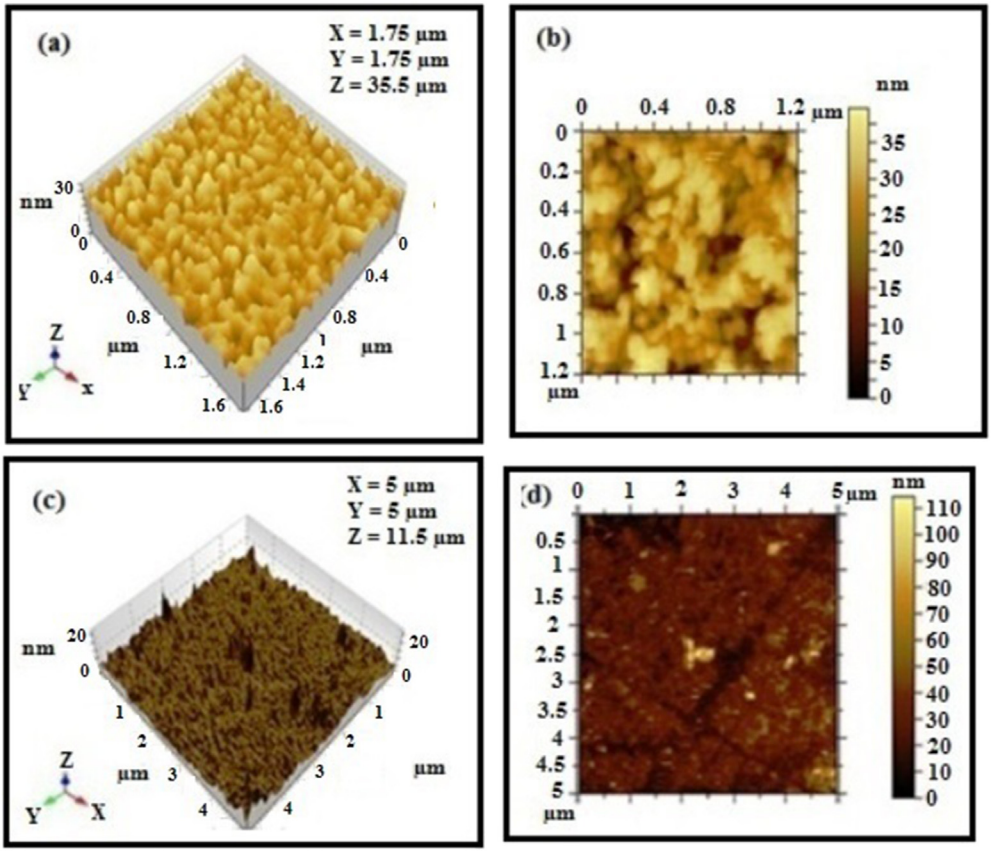

Fig. 7. AFM (a) 3D and (b) topographic images of unmodified TiO_2 NPs and AFM (c) 3D and (d) topographic images of modified TiO_2 NP.

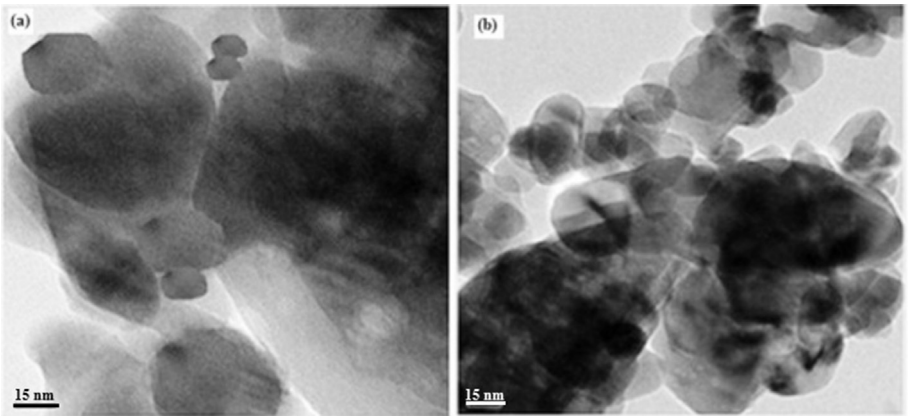

Fig. 8. TEM images of (a) Unmodified TiO_2 NPs, (b) Modified TiO_2 NPs.

3.5. FTIR characteristics of TiO_2–APTES–DGEBA nano-hybrid coatings

FTIR spectra of the unmodified and APTES grafted TiO_2 loaded epoxy nano-hybrid coatings are shown in Fig. 9. The spectra of the nano-hybrid coatings with different wt% surface modified TiO_2 nanoparticles contents exhibit the characteristic absorption peaks corresponding to polymeric groups and nanoparticles. It is evident that the peak intensity at 910 cm^{-1} corresponding to epoxide group significantly decreases after the silane modification, which indicates that the epoxide was chemically consumed by silane agent. It is also clear that the peak intensity of –OH at 3460 cm^{-1} increases due to the formation of new hydroxyl groups after the open-ring reaction of epoxide group. The appearance of the peak at 2920 cm^{-1} and 2852 cm^{-1}, 1017 cm^{-1} corresponding to –Si–O–CH_2–CH_3 and –Si–O– indicates that the silane component was grafted to epoxy resin. The incorporation of different nanoparticles in epoxy matrix caused slight changes in the intensities of absorption bands as well as the formation of new absorption bands in the range of 600–400 cm^{-1} which are attributed to the Ti–O stretching. This result confirmed the existence of TiO_2 nanoparticles in epoxy nano-hybrid coatings.

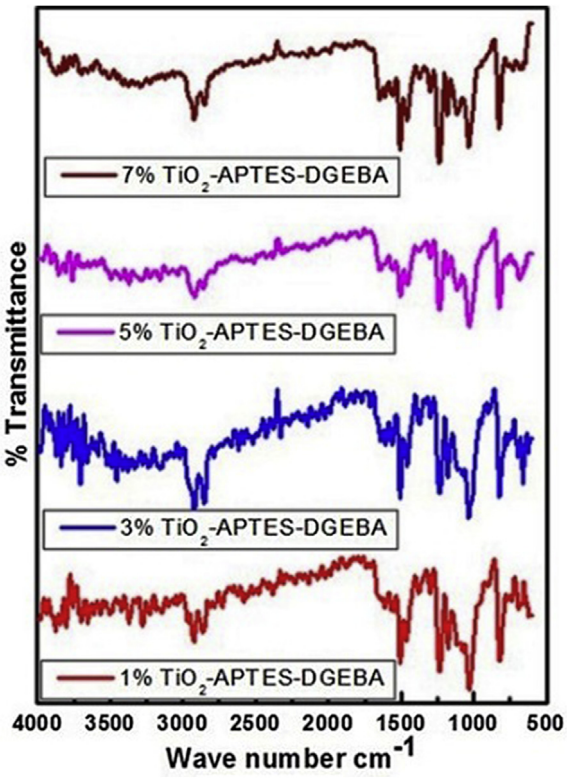

Fig. 9. FTIR spectra of Coating 'C1' (1%), Coating 'C2' (3%), Coating 'C3' (5%) and Coating 'C4' (7%).

3.6. SEM analysis of TiO_2–APTES–DGEBA nano-hybrid coatings

From these images (Fig. 10a&b), it was found that the surface modified different nanoparticles with coupling agent are spherical in shape. The results showed that all nanoparticles were homogeneously dispersed in epoxy matrix. The unmodified TiO_2 aggregated, and a crack around the aggregation emerged in the coating after, because there was no grafted epoxy resin on the TiO_2 surface, the compatibility between TiO_2 and epoxy resin was poor and interface bonding between nanoparticles and epoxy resin was weak. With the increasing of the graft density, the compatibility and interface bonding between nanoparticles and epoxy resin were improved; the aggregation of TiO_2 and the cracks around the aggregation were decreased. When the TiO_2 with the maximum graft density on the surface was added into the coating, few TiO_2 agglomerations and no cracks between the interface of nanoparticles and epoxy matrix were observed. Therefore, the compatibility and interface bonding between nanoparticles and epoxy resin were improved with the increase of graft density on the surface of nanoparticles. As it can be observed, for sample containing untreated nanoparticles, relatively large particle aggregates with a non-uniform distribution appeared on the surface of the samples. However, with APTES treatment of TiO_2 nanoparticles, the size of particle aggregates on the surface of the coating film minimum and more uniform distribution of nanoparticles was also achieved, as compared to its untreated counterparts. However, in order to evaluate the homogeneity and distribution of the nanoparticles to the entire volume of the film, further studies are needed.

3.7. Corrosion analysis of TiO_2–APTES–DGEBA nano-hybrid coatings by salts spray test

Fig. 10 shows the results of the 3.5% NaCl solution salts spray tests after 1200 h exposure. All the coatings tested exhibited the initial formation of corrosion products, which were inevitable, given their relatively thin nature. The coating under investigation is made using epoxy resin which forms one layer of coating system compared to other resins. Although the visual evaluation associated

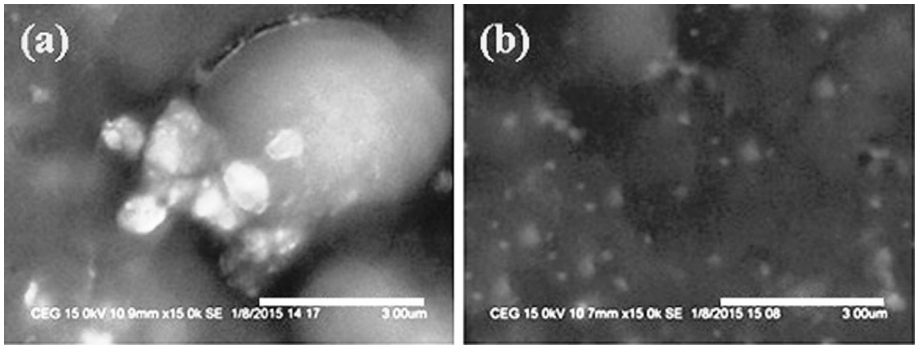

Fig. 10. SEM images of nanohybrid coatings (a) Unmodified TiO_2/DGEBA, (b) Modified TiO_2/DGEBA.

with this corrosion monitoring technique precludes differentiation between the 1, 3, 5 and 7 wt% TiO_2–APTES modified samples, those containing 'C2' (3 wt%) and 'C3' (5 wt%) TiO_2 appeared to be more corrosion resistant (Table 3). A similar trend was apparent after 1200 h, as shown in Fig. 11, with the 'C2' (3 wt%) and 'C3' (5 wt%) TiO_2 modified samples displaying the least white rust. After 1200 h, the corrosion of the epoxy layer had proceeded and all the samples then showed evidence of corrosion of the underlying steel, shown in Fig. 11. Considering the total corroded area as a measure of corrosion resistance, the 'C2' (3 wt%) TiO_2 sample remained the most effective, while that containing 'C1' (1 wt%) appeared to be satisfactory than the 'C0' (0 wt%) and 'C4' (7 wt%) concentrations over longer immersion. The test demonstrates that the addition of TiO_2 to the epoxy resin can have a positive effect on the corrosion resistance of the coating.

3.8. Corrosion analysis of TiO_2–APTES–DGEBA nano-hybrid coatings by EIS test

The epoxy coatings based on untreated and APTES–TiO_2 were subjected to accelerated corrosion test using an electrochemical impedance analysis. The Bode plots for the coating systems 'C1', 'C2', 'C3' and 'C4' are depicted respectively in Fig. 12. The values of impedance of all the coating systems are in between 4.93×10^8 and 1.27×10^6 Ω cm^2, exhibiting their excellent corrosion resistance. The corrosion resistance and phase angle θ value of the coating obtained are also presented in Table 4. It was clearly evident that the coating 'C3' (3 wt% of nano TiO_2) having high corrosion resistance value of 4.93×10^8 is superior to other coatings ('C1', 'C2', 'C3' and 'C4') with APTES–TiO_2. This superior corrosion resistance offered by coating system 'C3' may be due to the presence of optimum wt% of surface modified nano TiO_2 and its uniform distribution within the epoxy coating, which offers a defect free coating of low porosity and high cross linking density and coating integrity. Grafting of the silane coupling agent was found so effective to modify the surface properties of TiO_2 nanoparticles from hydrophilic to hydrophobic character by improving its dispersibility in epoxy nano-hybrid coatings. This clearly showed that proper interaction between matrix and the inorganic components would have occurred. The APTES–TiO_2 being uniformly dispersed throughout the film apparently serves to increase the hydrophobicity of the coating, by repelling water and corrosion initiators and thereby offering improved corrosion protection properties. This shows that APTES–TiO_2 containing coating is more protective in nature. The very high resistance values, i.e. $>10^8$ Ω cm^2 of all coatings of our present study indicate their high corrosion protection ability. On comparing the resistance values of TiO_2 containing coatings 'C1–C4' (3 wt% TiO_2) coating 'C2' exhibited the highest corrosion resistance values 4.93×10^8. The high values of resistance in the order of 10^8 Ω cm^2 obtained from Bode plots confirm that there was no contact between the electrolyte and metal substrate and suggest their excellent corrosion protection to steel surfaces. However, the resistance value is decreased slightly from the initial value of 4.93×10^8 Ω cm^2 to 3.88×10^7 after 30 days of immersion in 3.5% NaCl solution. Phase angle (theta) at high frequencies was recently considered as a useful parameter for evaluating the protective performances of nano hybrid coatings. If the coating shows high resistance, the current prefers to pass through dielectric pathways and the results will be higher phase angles (near 100°) between the current and the voltage. In low resistance coatings,

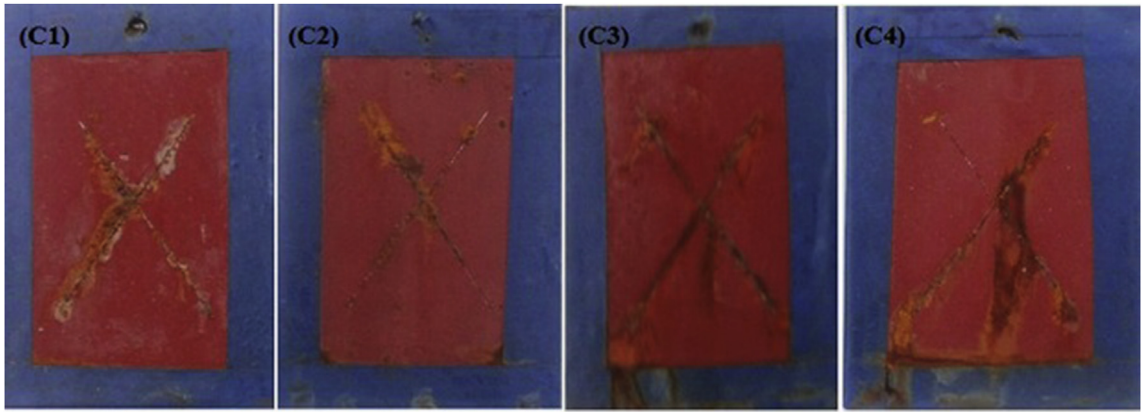

Fig. 11. The photographs of salt-spray exposed TiO_2–APTES–DGEBA coating samples for 1200 h.

Table 3
Results of salt spray test of TiO_2–APTES–DGEBA nano-hybrid coatings after 1200 h exposure of 3.5% NaCl.

Sample ID	Observation after 1200 h
C1	Light brown rust along the scribes, rust creep 2.5 mm along scribes
C2	No light brown rust along the scribes, rust creep 0.5 mm along scribes
C3	Light brown rust along the scribes, 1 mm along scribes
C4	Light brown rust along the scribes, rust creep 2 mm along scribes

Table 4
Data resulted from EIS analysis of 0 and 30 days of immersion in 3.5% NaCl.

Sample ID	Name of nanohybrid	NPs wt%	0 day immersion in 3.5% NaCl		30 days immersion in 3.5% NaCl	
			Impedance (Ω cm^2)	Theta (θ)	Impedance (Ω cm^2)	Theta (θ)
C1	TiO_2–APTES –DGEBA	1	1.15×10^7	75	1.27×10^6	71
C2		3	4.93×10^8	95	3.88×10^7	85
C3		5	1.71×10^8	90	1.52×10^7	86
C4		7	1.00×10^8	85	1.44×10^7	91

current prefers to pass through conductive pathways and the results are lower phase angles (near 0°). The phase angle plots of various coating systems 'C1', 'C2', 'C3' and 'C4' of present study are depicted in Fig. 12 for 0 and 30 days of immersion in 3.5% NaCl solution. Table 4 gives the values of phase angle θ measured for all coating systems on exposure to electrolyte solution for 0 and '30' days respectively. It shows that the phase angle of epoxy nano-hybrid coating 'C3' decreased during 30 days of the immersion from 95° to 85°. It can be concluded that this coating demonstrated capacitive behavior and that the coating was stable during the immersion time.

3.9. Protection mechanism of TiO_2–APTES–DGEBA nano-hybrid coatings

The corrosion resistance of APTES grafted TiO_2 epoxy coatings was superior than the corrosion resistance offered by unmodified TiO_2 grafted epoxy coating. Fig. 12 illustrates the impedance analysis of APTES grafted TiO_2 epoxy nano-hybrid coating compared with that of neat epoxy coatings. Table 4 gives a comparison between the impedance values of modified TiO_2 (3 wt%) epoxy coating with that of neat epoxy to find out the extent of reduction in corrosion. It can be seen that corrosion rate of modified TiO_2 epoxy coating is 4.3×10^8 Ω cm^2 while that of neat epoxy coating is found to be 3.21×10^4 Ω cm^2 indicating the excellent resistance against corrosion imparted by modified TiO_2 epoxy coatings. The modified TiO_2 (3 wt%) being uniformly dispersed throughout the film apparently serves as nano-structured cross-linking sites [21] to form hard protective films with high cross-link density and relatively [22] increase the hydrophobicity of the coating, by repelling water and corrosion initiators with an improved corrosion protection properties [23]. In contrast to this observation, modified TiO_2 coating containing 7 wt% exhibited inappropriate dispersion forming aggregates, air pockets as well as discontinuity of the film, which resulted in decrease in corrosion resistance.

3.10. Antibacterial behavior of TiO_2–APTES–DGEBA nano-hybrid coatings

TiO_2 is widely utilized as a self-cleaning and self-disinfecting surface coating material. TiO_2 has a more helpful role in environmental purification due to its photo induced super-hydrophobicity and antifogging effect [24]. These properties were applied in removing bacteria and harmful organic materials from water and air, as well as in self-cleaning or self-sterilizing surfaces in medical centers [25]. Some antimicrobial agents are extremely irritant and toxic and current researches are focused on formulate new types of safe and cost-effective biocide materials [26]. On the other hand, nano structured reservoirs made of inorganic oxides like TiO_2, and synthesized by the sol–gel process, were demonstrated to be biocompatible and suitable supports for a wide variety of compounds [27]. Therefore, in this study the effect of TiO_2–APTES nanoparticles was investigated against different microbes. The antimicrobial activity of TiO_2–APTES–DGEBA nanohybrid coatings was investigated against *Staphylococcus aureus* and *Pseudomonas aeruginosa* bacteria by zone inhibition method. Fig. 12 explains assessment of the antibacterial activity of TiO_2–APTES–DGEBA nanohybrid coatings with the concentration of TiO_2. Fig. 12a and b shows the activity against *S. aureus* and *P. aeruginosa* respectively. The results of zone inhibition method were described from Fig. 13a. It clearly shows that TiO_2 modified epoxy nanohybrid composite films show good inhibition zone around the films. It can be seen from Fig. 13a that the zone of inhibition increases with increase of TiO_2 concentration in epoxy nano-hybrid coatings. Fig. 13b and c clearly depicts that TiO_2 nanoparticles did not significantly reduce the growth of *P. aeruginosa* and *Aspergillus niger* strains. It is clearly

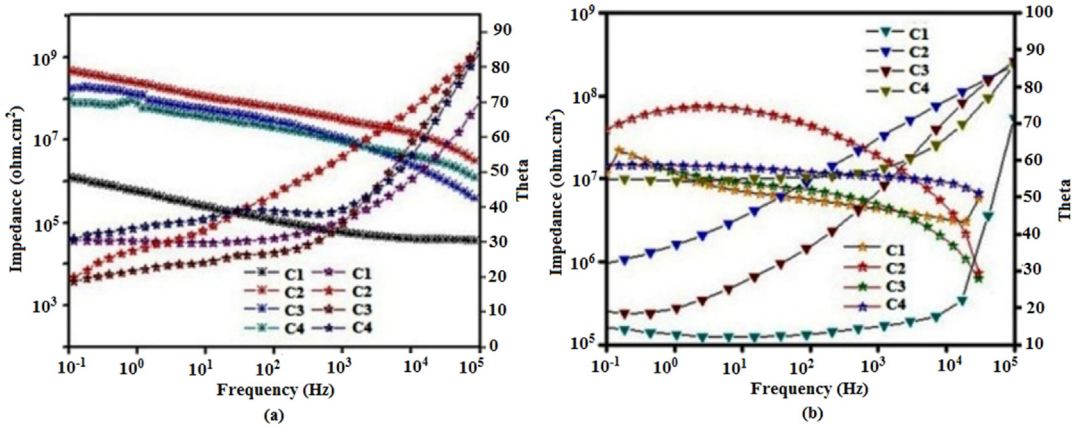

Fig. 12. Bode plot of TiO_2–APTES–DGEBA coating systems for (a) 0 days, (b) 30 days of immersion in 3.5% NaCl solution.

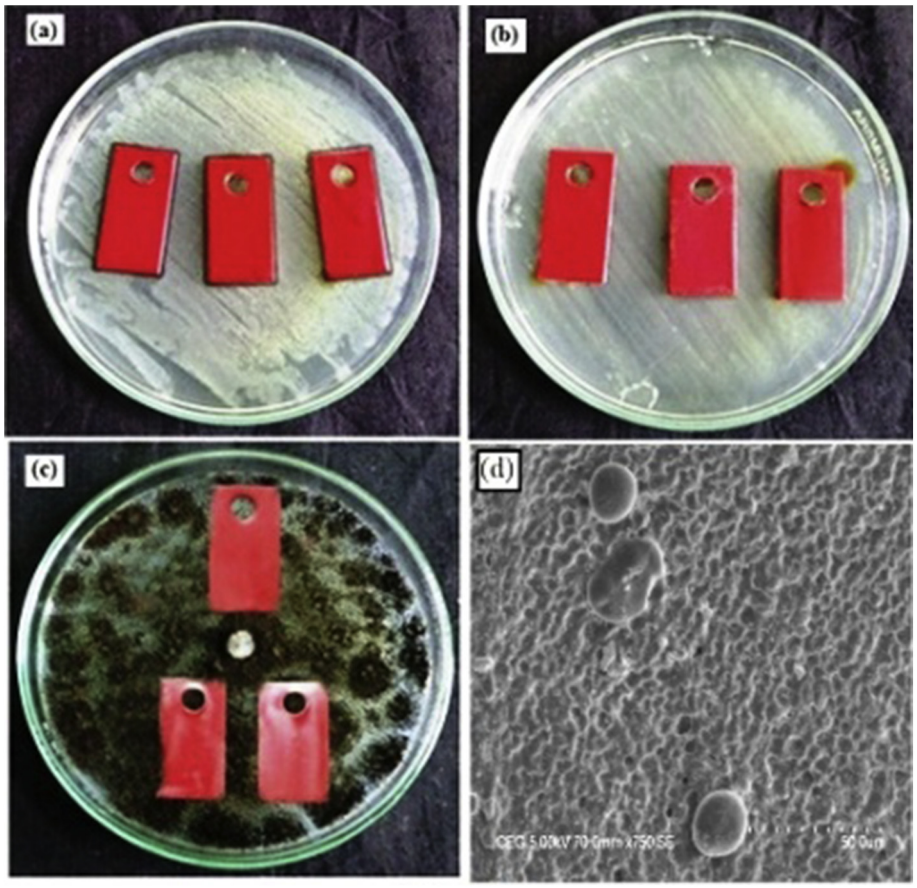

Fig. 13. Antimicrobial activities of TiO_2–APTES–DGEBA nanohybrid coatings against (a) *S. aureus*, (b) *P. aeruginosa*, (c) *A. niger* and (d) SEM image of *S. aureus* after treatment.

evident from the result that the antibacterial activity of the samples was notably stronger against Gram-positive *S. aureus* than Gram-negative *P. aeruginosa* [27]. The stronger antibacterial activity against Gram-positive bacteria is due to the structural difference in cell wall composition of Gram-positive and Gram-negative bacteria. The Gram-negative bacteria have a layer of lipopolysaccharides on the exterior, followed underneath by a layer of peptidoglycan. Furthermore, this structure helps bacteria to stay alive in environment where external materials exist that can damage them. The results of antibacterial activity of non-functionalised TiO_2 and TiO_2–APTES nanoparticles from the agar well diffusion method showed a remarkable inhibitory activity against *S. aureus*. This activity was caused due to Ti^{2+} ions on the surface bind to sulfur and phosphorus containing bio-molecules such as DNA or other biological moieties, thereby potentially causing cell damage. On the other hand, the antimicrobial capability of APTES–TiO_2 nanoparticles might be referred to their small size which is 250 times slighter than bacteria. This creates them stress-free to adhere with the cell wall of the microorganisms causing its destruction and leads to the loss of the cell. Fig. 13d visualizes the SEM image of destruction and cell death of *S. aureus* after exposure to APTES–TiO_2–DGEBA nanohybrid coatings. This observation further supports that APTES–TiO_2 nanoparticles may interact with *S. aureus* cells more efficiently. Also, the particles interact with the building elements of the outer membrane and might cause structural changes, degradation and finally cell death. This may be due to the suspension stability of APTES–TiO_2 is better in epoxy coatings. These observations further support the results of dispersion stability study. The SEM image shows that the surface modification significantly reduced nano aggregation and nano-size particles were resided on bacterial surface. After TiO_2 nanoparticles were surface modified, the individual nanoparticles or small-sized aggregated particles were tightly attached on the cellular surface, which may serve as a Ti^{2+} carrier and enhance the transport of toxic Ti^{2+} across extracellular polymeric substances and cell walls. Therefore, the TiO_2 anti-microbial activity, resulting from the surface modification process, was enhanced by the synergistic influence of particle's physical effect combined with the Ti^{2+} stresses.

3.11. Antifouling behavior of TiO_2–APTES–DGEBA nano-hybrid coatings

TiO_2 is a white powder with high opacity, brilliant whiteness, excellent covering power and resistance to color change. These properties have made it a valuable pigment and opacifier for a broad range of applications in paints. The antifouling properties of resins were investigated through a simple visual observation of the immersed coated panels and also verified the erosion and adhesion properties by visual inspection. Only two samples of our present study '(C2)' 3 wt% TiO_2–APTES and '(C3)' 5 wt% TiO_2–APTES were selected for comparing the antifouling properties of the resins. Sample '(C2)' showed the highest anticorrosion and antimicrobial activity between the two. The pictures corresponding to the antifouling test carried out in Bay of Bengal (Muttukadu) for 6 months of immersion are illustrated in Fig. 14, which shows that all samples except neat epoxy coated MS panel were free from erosion. Epoxy coated MS panel was covered by various types of marine fouling, including juvenile barnacles, oysters, polycheates and a thin slime

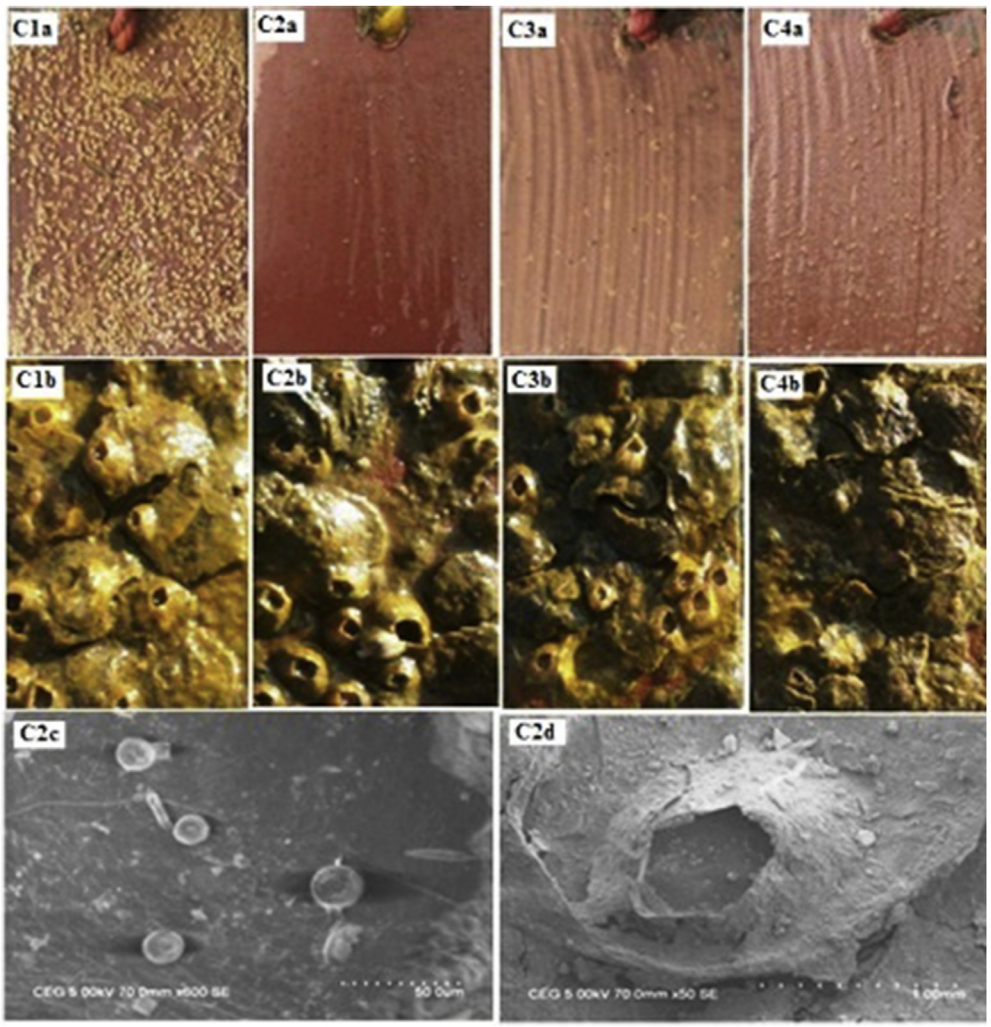

Fig. 14. Photograph taken after the TiO_2–APTES–DGEBA coated panels were immersed in seawater: (a) After 6th month, (b) After 12th month and SEM images taken (c) After 6th month, (d) After 12th month.

of an algal mat besides a heavy macro-fouling growth observed on this sample. However, the sample "C2" exhibited a greatly improved foul release behavior compared to other coating formulations. This is explained by the presence of silane functionalized TiO_2 (TiO_2–APTES) group, which protected the surface from the settlement of fouling organisms. The examined foul release coating developed in our present study consists only of the TiO_2–APTES loaded epoxy polymer resins unlike the commercial marine paint, which mainly consists of polymer resins, pigments, additives and organic solvents. Thus the TiO_2–APTES loaded epoxy nano-hybrid coatings with an optimum addition of 3 wt% TiO_2 can be more effective as foul release paint formulation with an improved antifouling property in comparison with the commercial antifouling paint formulation that consists of many harmful additives. Thus the TiO_2–APTES loaded epoxy nano-hybrid coating is environment friendly as well.

4. Conclusions

The corrosion resistance for various nano-hybrid coatings were in the following order 'C2' > 'C3' > 'C4' > 'C1' > 'C0' > MS. At the end of the salt spray test, no visible corrosion products were seen on the surface of the unscratched area of panels coated with modified epoxy coating containing 3 wt% surface modified TiO_2. This may be due to the APTES grafted TiO_2 nanoparticles, which can firmly adhere over the MS showed excellent corrosion resistance and thus no coating defects were found over the surface of the panels. This same order was retained from the results got from EIS. It was interesting to note that with the exception of the uncoated mild steel and mild steel with neat coating, all modified epoxy coated samples with TiO_2–APTES showed corrosion resistance up to $10^8\ \Omega\ cm^2$ indicating an excellent corrosion resistance. The superior corrosion resistance offered by coating system 'C2' may be due to the optimum wt% loaded TiO_2 nano particle and even its distribution within the epoxy matrix, which gave a flawless coating of low porosity, high cross linking density and improved coating integrity. For the investigation of the antimicrobial behavior, the plates coated with nano-hybrid epoxy were treated with microorganisms. The outcome of zone inhibition test indicated that the antimicrobial activity of various nano-hybrid coatings. The use of TiO_2–APTES exhibited the highest effect on *S. aureus* microorganisms due to the progressed surface chemistry and chemical stability of TiO_2–APTES which make them easy to interact with the bacteria. The particles also interact with the building elements of the outer membrane and cause structural changes, degradation and finally cell death to bacteria. The results expressed that the antifouling efficiency of the coating film first is improved by adding 3 wt% of TiO_2–APTES and then the performance becomes worse when the amount of

TiO_2–APTES reached is 5 wt% and 7 wt% respectively. The reason which caused this change of antifouling property may be inferred as follows. When the addition of TiO_2–APTES is 3 wt%, it is well distributed within the coating, to effectively inhibit bio-fouling. On the other hand, if the addition of TiO_2–APTES is beyond 3 wt%, the excess addition causes uneven distribution of TiO_2–APTES in the coating film which might have led to the pore formation on the surface of the coating namely 'C3' and 'C4'.

References

[1] T. Mochi, Phase structure and thermomechanical properties of primary and tertiary amine-cured epoxy/silica hybrids, J. Polym. Sci. Part B Polym. Phys. 39 (2001) 1071–1084.

[2] M. Okazaki, M. Murota, Y. Kawaguchi, Curing of epoxy resin by ultrafine silica modified by grafting of hyperbranched polyamidoamine using dendrimer synthesis methodology, J. Appl. Polym. Sci. 80 (2001) 573–579.

[3] C. Gao, Effects of nanometer material and their application, J. Jiangsu Univ. Sci. Technol. 22 (2001) 63–70.

[4] G.P. Bierwagen, Reflections on corrosion control by organic coatings, Prog. Org. Coat. 28 (1996) 43–48.

[5] K. Lam, K.T. Lau, Localized elastic modulus distribution of nanoclay/epoxy composites by using nanoindentation, Compos. Struct. 75 (2006) 553–558.

[6] G. Shi, M.Q. Zhang, M.Z. Rong, B. Wetzel, K. Friedrich, Friction and wear of low nanometer Si_3N_4 filled epoxy composites, Wear 254 (2003) 784–796.

[7] M.S. Hartwig, D. Putz, L. Aberle, Preparation, characterisation and properties of nanocomposites based on epoxy resins – an overview, Macromol. Symp. 221 (2005) 127–136.

[8] F. Dietsche, Y. Thomann, R. Thomann, R. Mulhaupt, Translucent acrylic nanocomposites containing anisotropic laminated nanoparticles derived from intercalated layered silicates, J. Appl. Polym. Sci. 75 (2000) 396–405.

[9] S. Suresh, P. Saravanan, K. Jayamoorthy, S. Ananda Kumar, S. Karthikeyan, Development of silane grafted ZnO core shell nanoparticles loaded diglycidyl epoxy nanocomposites film for antimicrobial applications, Mater. Sci. Eng. C 64 (2016) 286–292.

[10] O. Becker, R. Varley, G. Simon, Morphology, thermal relaxations and mechanical properties of layered silicate nanocomposites based upon high-functionality epoxy resins, Polymer 43 (2002) 4365–4373.

[11] L.H. Yang, F.C. Liu, E.H. Han, Effects of P/B on the properties of anticorrosive coatings with different particle size, Prog. Org. Coat. 53 (2005) 91–98.

[12] S.V. Umaka, M.L. Zheludkevich, K.A. Yasakau, R. Serra, S.K. Poznyak, M.G.S. Ferreira, Nanoporous titania interlayer as reservoir of corrosion inhibitors for coatings with self-healing ability, Prog. Org. Coat. 58 (2007) 127–135.

[13] V. Palanivel, D. Zhu, W.J. Van Ooij, Nanoparticle-filled silane films as chromate replacements for aluminum alloys, Prog. Org. Coat. 47 (2003) 384–392.

[14] W.J. Van Ooij, D. Zhu, Electrochemical impedance spectroscopy of bis-(triethoxysilypropyl)tetrasulfide on Al 2024-T3 substrates, Corrosion 57 (2001) 413–427.

[15] M.G.S. Ferreira, R.G. Duarte, M.F. Montemor, A.M.P. Simoes, Silanes and rare earth salts as chromate replacers for pre-treatments on galvanised steel, Electrochim. Acta 49 (2004) 2927–2935.

[16] J.D. Adkins, A.E. Mera, M.A. Roe-Short, G.T. Pawlikowski, R.F. Brady, Novel non-toxic coatings designed to resist marine fouling, Prog. Org. Coat. 29 (1996) 1–5.

[17] O. Iguerb, C. Poleunis, F. Mazeas, C. Compere, P. Bertrand, Antifouling properties of poly(methyl methacrylate) films grafted with poly(ethylene glycol) monoacrylate immersed in seawater, Langmuir 24 (2008) 12272–12282.

[18] L. Shtykova, C. Fant, P. Handa, Adsorption of antifouling booster biocides on metal oxide nanoparticles: effect of different metal oxides and solvents, Prog. Org. Coat. 64 (2009) 20–26.

[19] H. Sakai, T. Kanda, H. Shibata, Preparation of highly dispersed core/shell-type titania nanocapsules containing a single Ag nanoparticle, J. Am. Chem. Soc. 128 (2006) 4944–4945.

[20] X. Xu, M. Oliveira, J.M.F. Ferreira, Effect of solvent composition on dispersing ability of reaction sialon suspensions, J. Colloid Interf. Sci. 259 (2003) 391–397.

[21] G. Li, G.L. Wang, H. Ni, C.U. Pittman, Polyhedral oligomeric silsesquioxane (POSS) polymers and copolymers. A review, J. Inorg. Organomet. Polym. 11 (2001) 123–154.

[22] D.K. Chattopadhyay, K.V.S.N. Raju, Structural engineering of polyurethane coatings for high performance applications, Prog. Polym. Sci. 32 (2007) 352–418.

[23] R. Zandi-zand, A. Langroudi, A. Rahimi, Organic–inorganic hybrid coatings for corrosion protection of 1050 aluminum alloy, J. Non-Cryst. Solids 351 (2005) 1307–1311.

[24] A. Fujishima, K. Honda, TiO_2 photoelectrochemistry and photocatalysis, Nature 238 (1972) 37–38.

[25] S. Tojo, T. Tachikawa, M. Fujitsuka, J. Majima, Iodine-doped TiO_2 photocatalysts: correlation between band structure and mechanism, J. Phys. Chem. 112 (2008) 14948–14954.

[26] H. Kato, A. Kudo, Visible-light-response and photocatalytic activities of TiO_2 and $SrTiO_3$ photocatalysts codoped with antimony and chromium, J. Phys. Chem. B 106 (2002) 5029–5034.

[27] A. Peterson, T. Lopez, I.E. Ortiz, R.D. González, Pore structures in an implantable sol–gel titania ceramic device used in controlled drug release applications: a modeling study,, Appl. Surf. Sci. 253 (2007) 5767–5771.